

Full Length Article

Correlations between the catalyst properties and catalytic activity of Au on ZrO₂-CeO₂ in the hydrogenation of CO₂Hue-Tong Vu^a, Matjaž Finšgar^b, Janez Zavašnik^c, Nataša Novak Tušar^{a,d}, Albin Pintar^{a,*}^a Department of Inorganic Chemistry and Technology, National Institute of Chemistry, Hajdrihova 19, SI-1001 Ljubljana, Slovenia^b Faculty of Chemistry and Chemical Engineering, University of Maribor, Smetanova 17, SI-2000 Maribor, Slovenia^c Gaseous Electronics, Jožef Stefan Institute, Jamova cesta 39, SI-1000 Ljubljana, Slovenia^d University of Nova Gorica, Vipavska ulica 13, SI-5000 Nova Gorica, Slovenia

ARTICLE INFO

Keywords:

CO₂ utilization
Au
CeO₂-ZrO₂ mixed oxides
Amorphous ZrO₂
Methanol synthesis

ABSTRACT

To exploit the potential of both ZrO₂ and CeO₂, the mixed oxides with Ce content up to 5 wt.% were prepared via the simple coprecipitation method, subsequently loaded with Au catalysts, and investigated in the hydrogenation of CO₂. The obtained catalysts, namely Au/ZrCe_x ($x = n_{\text{Ce}}/n_{\text{Zr}} = 0.0\text{--}0.1$), exhibit similar Au content (0.7 wt.%), structural and textural properties, however, considerably different acidic/basic properties and great surface oxygen vacancy. The introduction of Ce leads to slightly decreased CO₂ conversion, which was found proportional to the Ce content. Interestingly, it is evidenced that the methanol selectivity is closely related to the acidic/basic properties of the catalysts employed. Over the broad range of acid site density (ASD) ranging from 400 to 700 μmol g⁻¹, the highest methanol selectivity of 27 % was recorded at 250 °C and 40 bar over the catalyst exhibiting an ASD of 600 μmol g⁻¹, which decreased with further increasing ASD. The volcano-shape trend was also discovered for the base site density showing the critical point at 120 μmol g⁻¹ over the range from 90 to 210 μmol g⁻¹. These findings suggest that the acidic/basic properties can be tuned, e.g., via thermal treatment, to tailor the product distribution of the CO₂ hydrogenation. Above all, the Au catalysts supported on ZrO₂-CeO₂ mixed oxides exhibit excellent catalytic stability, e.g., a methanol formation rate of 3.32 g_{CH₃OH} • (g_{Au} • h)⁻¹ remained over the reaction course of 93 h at 250 °C and 40 bar for Au/ZrCe_{0.025} sample.

1. Introduction

Facing one of the acute environmental crises, i.e., global warming that is attributed mainly to the massive CO₂ emission via the combustion of fossil fuels, more and more efforts from both industrial and academic researchers have been made to reduce atmospheric CO₂ or, even better, to transform it into value-added chemicals and thus advocate a circular carbon economy. CO₂ can be utilized as a promising carbon feedstock for various functional molecules, e.g., methanol [1,2], higher alcohols [3,4], dimethyl ether [5] and C₂₊ hydrocarbons [6–8]. The transformation of CO₂ into methanol, which is well recognized as an important bulk chemical in industries [9,10], is of interest in this study. In general, the activation of CO₂ molecules remains a challenge in CO₂ conversion due to its notorious high thermodynamic stability ($\Delta H_f^0 = -393.5 \text{ kJ mol}^{-1}$) [11]. Moreover, the methanol synthesis from CO₂ is known from the literature to undergo a competition with the reverse water gas shift (RWGS) reaction forming CO and possibly the conversion

of CO into methanol [12]. While RWGS is endothermic, the methanol synthesis is exothermic ($\Delta H^0 = -49.5 \text{ kJ mol}^{-1}$) and thermodynamically unfavored at high temperatures [10,13]. Therefore, catalysts are crucial to lower the activation energy and consequently enhance the yield of methanol in the thermocatalytic conversion of CO₂. Alternatively, CO₂ can be converted using various approaches, including molecular catalysis [14], photocatalysis, electrocatalysis [15] and hybrid approaches [16], which are out of the scope of this study.

There have been numerous attempts to improve the catalytic activity via catalyst design. Regarding the active metals, three main groups have been studied extensively, namely, Au-, Pd- and Cu-based catalysts, besides other metals (Pt, Ni, Co, Ru, ...) [5,12,14]. The selection of catalysts is further extended to bimetallic [17] and trimetallic catalysts [18] in order to advance the synergy of the multicomponent catalytic systems. Irrespective of active metals employed, the particle size and the dispersion of active metals were found crucial to the catalytic performance in the hydrogenation of CO₂. In particular, the increase of Cu

* Corresponding author.

E-mail address: albin.pintar@ki.si (A. Pintar).<https://doi.org/10.1016/j.apsusc.2023.156737>

Received 12 December 2022; Received in revised form 9 February 2023; Accepted 10 February 2023

Available online 14 February 2023

0169-4332/© 2023 The Author(s). Published by Elsevier B.V. This is an open access article under the CC BY-NC-ND license (<http://creativecommons.org/licenses/by-nc-nd/4.0/>).

particle size (5–25 nm), in association with gradual raising Cu content (5–25 wt.%) supported on CeO₂-ZrO₂ materials, leads to a reduction in the number of active Cu sites exposed to reactants, as indicated by lower H₂ consumption during temperature programmed reduction, and thus lower methanol formation activity (from 2.92 to 0.46 $g_{CH_3OH} \cdot (g_{Cu} \cdot h)^{-1}$) [19]. Similar observations are also recorded for Cu-based catalysts supported on various types of materials, e.g., CeO₂ [20], Al₂O₃ [21], ZnO [22], and ZrO₂ [23]. Au-based catalyst is another classic example of the strong dependence between Au particle size and the corresponding catalytic activity [24–26]. The highly dispersed Au nanoparticles (≈ 1 nm) supported on amorphous ZrO₂ via deposition precipitation method provided a much higher methanol formation rate than that of Au/ZrO₂ ($d_{Au} \approx 50$ nm) synthesized by impregnation, i.e., $2.1 > 0.4 g_{CH_3OH} \cdot (g_{cat} \cdot h)^{-1}$ in the methanol synthesis from CO₂ (240 °C, 40 bar) [27]. It is suggested that the particle size of active metal is strongly associated to the number of interfacial surface area, at which the methanol synthesis has been repeatedly reported to take place [28,29]. Hence, the high specific surface area of interfacial sites can promote the hydrogenation of CO₂ into methanol and thus lower the formation of CO.

Besides, there are other factors affecting the catalytic performance of solids, in particular, reducibility indicated by the temperature at which most of the active metal is reduced, the chemical nature of active sites and the corresponding role of each site, and active sites dispersion determined by the specific surface area of support materials as well as the interaction between the metals and supports. Therefore, one of the approaches to improve the catalytic performance is via support materials.

Regarding the support materials, there are a plethora of choices, among these, γ -Al₂O₃, ZnO, CeO₂, ZrO₂, SiO₂, TiO₂, and mixed oxides of various rare-earth and transition metals are widely studied in the hydrogenation of CO₂. One of the key roles of these materials is providing high surface area and thus improving the dispersion of the active metals. Besides, the acid-base properties of the catalyst support are also required to influence the catalytic activity of CO₂ conversion greatly. The catalysts supported on acidic materials (TiO₂, ZrO₂) are beneficial for CO₂ conversion [30,31], which is contributed mainly by the RWGS reaction forming CO, whereas methanol formation is favored over catalysts exhibiting strong basic properties (CeO₂, ZnO) coupled with low CO₂ conversion [31–33]. The different behaviors were speculated to associate with the high basicity, which reinforced the adsorption of CO₂ and CO, thereby stabilizing the formate intermediates to methanol and possibly hindering the production of by-product CO, respectively [34]. Moreover, acidity caused by Cu cations adjacent to oxygen vacancies was found to be linear with the methanol formation rate [35]. However, further understanding, particularly the influencing manner of these basic/acidic sites in CO₂ hydrogenation, remains debatable. Furthermore, the combination of different metal oxides, particularly CeO₂-ZrO₂ mixed oxides, has shown numerous benefits, including greater dispersion, reducibility, and interaction between metallic sites, e.g., Cu and support [33,36–38]. Taking into consideration, for example, the Au-based catalysts on TiO₂, due to the electronic polarization between Au and the support only observed in the presence of CeO₂, both CO₂ adsorption and activation were greatly improved [39]. Additionally, the surface hydroxyl groups available on metal oxides were found to participate in the surface chemical reaction and affect the selectivity of CO₂ conversion into methanol. These groups were found to promote the adsorption of CO₂ at the isolated Cu sites in proximity resulting in bidentate formate, the primary reactive intermediate of methanol synthesis, for urea-assisted hydrothermally synthesized Cu/SiO₂ [40]. Another study combining experimental and theoretical results for SiC quantum dots revealed that the hydroxyl groups lowered the barrier to form formate intermediates and thus increased the methanol productivity [41]. This phenomenon was also observed in various catalytic systems, e.g., Rh-based catalysts supported on TiO₂ [42] and Cu/ γ -Al₂O₃

[43]. These are a few factors important for methanol synthesis, apart from the morphology of the supports [23,44–48], which are not discussed in detail. Nevertheless, the changes in catalytic activity seem to be under the influence of multiple factors. Thus, one should consider all possible reasons and their corresponding gravity to obtain a full spectrum based on which solid conclusions can be drawn.

In our study, the objective was to exploit the advantages of Ce, i.e., great basicity and surface oxygen vacancy, in Au catalysts supported on amorphous ZrO₂ (a-ZrO₂) for CO₂ hydrogenation. Owing to the great number of uniform acidic sites mainly contributed by Lewis acid sites and a fraction of surface hydroxyl groups as reported in [49], a-ZrO₂ was chosen over monoclinic (m-) and tetragonal (t-) ZrO₂, two commonly found phases of ZrO₂. Furthermore, CeO₂-ZrO₂ mixed oxides were obtained by a simple and low-energy cost coprecipitation method, which is highly desired amid the current energy crisis [27]. Accordingly, a series of Au catalysts supported on CeO₂-ZrO₂ mixed oxides with a gradually increased molar ratio of Ce to Zr (from 0 to 0.1, with a step of 0.025) was prepared. The gradual increase of Ce content offers a systematic approach to investigating the influence of Ce on the properties of the resulting catalysts based on a-ZrO₂. Furthermore, the catalytic activity of the Au-based catalysts supported on CeO₂-ZrO₂ mixed oxides in the hydrogenation of CO₂ into methanol was examined and elucidated by considering various influential factors, e.g., reducibility, acid-base properties, chemical environment (of Au, Ce, Zr), and Au particles size of the catalysts.

2. Experimental

2.1. Synthesis of ZrO₂-CeO₂ mixed oxides

The ZrO₂-CeO₂ nanocomposites were synthesized following a precipitation method in a previously published work [27] with slight adjustments. Typically, 4 g of zirconium (IV) oxynitrate (ZrO(NO₃)₂·xH₂O, Sigma Aldrich) and a predetermined amount of cerium (III) nitrate hexahydrate (Ce(NO₃)₃·6H₂O, Sigma-Aldrich) was dissolved in 50 mL deionized water resulting in an aqueous solution of 0.1 M Zr⁴⁺ and 0.1x M Ce³⁺, respectively, with x denoted for the Ce to Zr molar ratios ($x = n_{Ce}/n_{Zr}$). To obtain high dispersion of Ce in ZrO₂, x was varied in the low range from 0.000 to 0.025, 0.05, 0.075 and 0.100. The mixture was stirred at room temperature (RT) for 30 min. Subsequently, the precipitation was conducted by adding 5 wt.% ammonia solution (pH = 12) dropwise (approximately 10 mL) to the Zr⁴⁺ and Ce³⁺ aqueous solutions (pH = 1–1.5) until complete precipitation (pH \approx 9). The mixtures were then placed in a dryer at 80 °C under static air for 12 h. Afterwards, the obtained mixtures were washed and filtered with deionized water. The solids were dried at 90 °C overnight and subsequently calcined at 300 °C under static air for 4 h. The obtained products are labelled as ZrCex with x referring to the nominal n_{Ce}/n_{Zr} ratio.

2.2. Introduction of Au by deposition precipitation

In order to obtain small Au particle size, which is favored at low Au content, a nominal Au content of 1 wt.% was chosen for Au introduction. Specifically, 1 g of ZrCex was added into 50 mL of 1 mM gold (III) chloride trihydrate (HAuCl₄·3H₂O, Sigma-Aldrich) aqueous solution. The suspension was stirred at room temperature (RT) for 30 min. The deposition precipitation was conducted by adding 5 wt.% ammonia solution (approximately 3 mL) in droplets until complete precipitation (pH = 7). The suspension was then transferred to a dryer, and the temperature was kept at 80 °C under static air for 6 h. Afterwards, the solids were filtered and washed with water. The obtained materials were further dried at 120 °C for 2 h and named as Au/ZrCex ($x = n_{Ce}/n_{Zr} = 0, 0.025, 0.05, 0.075$ and 0.1).

2.3. Catalyst characterization

The structural properties of all investigated catalysts were characterized by a PANalytical X'Pert PRO MPD X-ray diffractometer (Cu $K_{\alpha 1}$ = 0.154 nm). The powder X-ray diffraction patterns were recorded at room temperature in the 2θ range from 5° to 90° with a step of 0.033° .

The elemental content of Au, Ce, and Zr in synthesized catalysts was determined by optical emission spectroscopy with inductively coupled plasma (ICP-OES) using a Varian 715-ES ICP Optical Emission Spectrometer. In preparation for the analysis, 10 mg of the samples were dissolved in 10.0 mL HF and 1.0 mL $HClO_4$ and diluted to obtain 50.0 mL aqueous solutions.

N_2 sorption isotherms were recorded on a volumetric adsorption analyzer Tristar 3000 (Micromeritics, Norcross (GA), USA) at 77 K. Prior to the measurements, the samples were evacuated at $180^\circ C$ for 10 h. The specific surface area (A_{BET}) and total pore volume (V_P) were determined using the Brunauer–Emmett–Teller (BET) model and single point ($p/p_0 = 0.98$) method, respectively.

Temperature-programmed reduction with H_2 (H_2 -TPR) was performed using a Micromeritics AutoChem II 2920 chemisorption analyzer. 60 mg of the catalysts was inserted into a U-shaped quartz tube and oxidized at $400^\circ C$ under 5 vol% O_2 in argon (Ar) (25 mL min^{-1}) for 10 min with a heating rate of 10 K min^{-1} . Subsequently, before the reduction of the samples, the gas line was switched to Ar (25 mL min^{-1}) for O_2 evacuation ($50^\circ C$, 10 min) followed by reducing the catalysts using the mixture of 5 vol% H_2 in Ar (25 mL min^{-1}) at a constant heating rate of 10 K min^{-1} up to $350^\circ C$. Hydrogen consumption was determined using a TCD detector and a calibration using Ag_2O (from Micromeritics) as a reference.

Temperature-programmed desorption with CO_2 (CO_2 -TPD) analyses were carried out using the aforementioned AutoChem II 2920 chemisorption analyzer (Micromeritics, USA) coupled with a mass spectrometer (Pfeiffer Vacuum, model ThermoStar). The samples were placed into a U-shaped quartz tube and reduced at $300^\circ C$ under 5 vol% H_2 in Ar (25 mL min^{-1}). The samples were then cooled down to $50^\circ C$ and flushed with Ar (25 mL min^{-1}) for 15 min. At the same temperature ($50^\circ C$), the reduced samples were saturated with 80 vol% CO_2 in Ar via 20 pulses of 0.532 mL. The average peak area of the last 15 pulses was used as the calibration for the quantification of CO_2 desorption. Subsequently, the samples were heated with a heating ramp of 10 K min^{-1} up to $400^\circ C$ under Ar (25 mL min^{-1}) for CO_2 desorption. The amount of desorbed CO_2 was determined via integration of the total area under the MS fragment $m/z = 44$.

The pyridine adsorption-desorption experiments were carried out using a Perkin Elmer Pyris 1 TGA instrument to determine the acid site density of reduced catalysts. The as-synthesized catalysts were reduced externally in a tubular oven at $350^\circ C$ in H_2 flow (50 mL min^{-1}) for 4 h. Subsequently, the samples were placed in a sample pan and pretreated at $350^\circ C$ in nitrogen flow (50 mL min^{-1}) for 30 min, then cooled down to $50^\circ C$ at which the sample weight was recorded and referred to as m_0 (g). The pyridine saturation step was carried out by flushing with pyridine vapor in nitrogen flow (50 mL min^{-1}) until recording a constant weight. The excess pyridine was removed by purging with nitrogen flow (50 mL min^{-1}) at $50^\circ C$ for 2 h. The temperature was then increased to $450^\circ C$, with a heating rate of 20 K min^{-1} . The desorption of pyridine was recorded via the sample weight loss as a function of temperature/time. The weight loss during the desorption of pyridine while heating from $50^\circ C$ to $450^\circ C$ is Δm (mg). Assuming the stoichiometry between pyridine molecule and acid site is equal to 1, the acid site density (ASD) was, therefore, calculated as follows $ASD = \frac{\Delta m}{M_{pyridine} \cdot m_0}$ ($\text{mmol} \cdot \text{g}^{-1}$) with $M_{pyridine} = 79.1\text{ g/mol}$.

The carbon content of the fresh and spent catalyst samples were determined using a 2400 series II CHNS elemental analyzer (Perkin Elmer, USA).

The crystallography, phase composition, morphology, and size of the

samples containing Au nanoparticles were analyzed by transmission electron microscope (TEM, JEM-2100, JEOL), operating at 200 kV and equipped with a high-resolution slow-scan CCD camera (Orius SC1000, Gatan). The powdered samples pre-reduced in a tubular oven (in the H_2 flow (40 mL min^{-1}) at $350^\circ C$ for 4 h) were dispersed in absolute ethanol and sonicated to prevent agglomeration. The suspension was transferred onto Cu-supported amorphous carbon grids. The maximum Feret diameter was used as the size descriptor of Au nanoparticles, which was manually outlined and determined using ImageJ. To obtain a representative overview of Au particles, the TEM micrographs were recorded at various sites of interest for each sample, and the number of particles detected is up to 150 particles. Before the TEM investigation, the microscope image and diffraction mode were calibrated by the MAG* I^* CAL * reference standard through all of the magnification ranges, with the overall uncertainty on the calibrated values $\Delta t < 1.0\%$.

X-ray photoelectron spectroscopy (XPS) measurements were performed with a Supra plus instrument (Kratos Analytical, Manchester, UK) equipped with an Al K_{α} excitation source and a monochromator. The measurements were performed with a spot size of $700 \times 300\ \mu\text{m}$. Pass energy of 160 eV and 20 eV were used to obtain a survey and high-resolution spectra, respectively. The binding energy scale was corrected using the C-C/C-H peak at 284.8 eV in the C 1s spectrum. The neutralizer was on during the spectrum acquisition. Data were acquired and processed using ESCApe 1.4 (Kratos, Manchester, UK). The background of the high-resolution spectra was subtracted according to the method of Shirley [50]. Reported atomic concentrations at the surface were normalized to 100.0%.

2.4. Catalytic hydrogenation of CO_2

The hydrogenation of CO_2 was carried out in a fixed-bed reactor (Microactivity Reference MA-Ref reactor from PID Eng&Tech, Madrid, Spain). Typically, an amount of ca. 200 mg of the catalysts was packed and sandwiched with quartz wool in a tubular reactor (I.D. = 9 mm, L = 305 mm) made of Hastelloy. During the packing step, the reactor was tapped frequently to ensure reproducible packing state of the catalyst beds. The catalysts were reduced internally using a mixture of H_2 (30 mL min^{-1}) and N_2 (10 mL min^{-1}) at $350^\circ C$ for 4 h. Afterwards, the reactor pressure was increased to 40 bar, and the temperature was reduced to $250^\circ C$. The reactant mixture comprised of CO_2 (24 vol%) and H_2 (72 vol%) balanced in N_2 (4 vol%). The gas flow rate was 40 mL min^{-1} (GHSV = 48000 h^{-1}). The steady state was typically reached after 1 h marking the start of the catalytic experiments. In each experiment, the product mixture was sampled every 20 min in 2 h. The remaining reactants and gas products in the discharged gas stream were analyzed using an online Agilent 7890A chromatograph equipped with Porapak Q, HayeSep Q and molecular sieve 5A columns. The CO_2 conversion (X_{CO_2}) and selectivity to methanol (S_{CH_3OH}) and CO (S_{CO}) were calculated using the following equations:

$$X_{CO_2} = \frac{n_{CO_2,in} - n_{CO_2,out}}{n_{CO_2,in}} \cdot 100\% \quad (1)$$

$$S_{CH_3OH} = \frac{n_{CH_3OH}}{n_{CO_2,in} - n_{CO_2,out}} \cdot 100\% \quad (2)$$

$$S_{CO} = \frac{n_{CO}}{n_{CO_2,in} - n_{CO_2,out}} \cdot 100\% \quad (3)$$

where $n_{CO_2,in}$ and $n_{CO_2,out}$ refer to the input and output molar amount of CO_2 . n_{CH_3OH} and n_{CO} are the molar numbers of methanol and CO, respectively, in the product mixtures. Based on the 6 collected data points, the average and standard deviation of X_{CO_2} , S_{CH_3OH} and S_{CO} were determined. Besides, the methanol formation rate (r_{CH_3OH}) was also used as a measure to evaluate the catalytic activity of the studied catalysts in the hydrogenation of CO_2 into methanol. The methanol formation rate (r_{CH_3OH}) was calculated as follows:

$$r_{CH_3OH} = \frac{Q_{CO_2} \cdot X_{CO_2} \cdot S_{CH_3OH} \cdot MW_{CH_3OH}}{m_{Au}} [g_{CH_3OH} \cdot (g_{Au} \cdot h)^{-1}] \quad (4)$$

where Q_{CO_2} , MW_{CH_3OH} and m_{Au} denote the total flow rate of the reaction mixture, the molecular weight of methanol, and Au mass of the catalysts, respectively.

3. Results and discussion

3.1. Catalyst characterization

The elemental composition of synthesized solids, namely, the content of Au, Ce, and Zr, was determined by the ICP-OES technique, and the results are displayed in Table 1. All the catalysts exhibit a comparable Au content of 0.7 wt.% lower than the nominal Au content (1 %), which is probably associated with the hydration of hygroscopic Au precursor. Additionally, the Ce content gradually increased up to 4.6 wt.% rendering a gain in the Ce to Zr molar ratio (n_{Ce}/n_{Zr}) from 0 to 0.09, which agrees well with the nominal n_{Ce}/n_{Zr} . The chlorine content was determined in Au-containing catalyst samples, after digestion, by using in-house ion chromatography method. In the analyzed samples, the content of chlorine was below the level of quantification, i.e. <0.5 mg/g.

3.1.1. Structural and textural properties

The structural properties of all the catalysts were characterized by XRD analysis, from which the results are shown exemplarily for Au/ZrCex samples in Fig. 1. Independently of Ce and Au content, all the samples exhibit almost identical XRD patterns featuring 2 broad signals centered at 2θ of 31° and 55° , which can be ascribed to a-ZrO₂. No other phases, e.g., cerium oxides and Au-containing phases, were detected. This might be explained by the low content of Ce and Au, or they are present in very fine particles below the detection limit of XRD. The latter was later excluded by TEM analysis. Specifically, the deposited Au is evidenced by TEM and selected area electron diffraction (SAED), which are exemplarily shown for Au/ZrCe0.05 in Fig. 2. The SAED pattern of the Au particle shows sharp and continuous rings corresponding to individual crystal planes. On the other hand, the ZrO₂-based support material exhibits a halo ring typical for amorphous materials and blurred rings indicating a short-range order (Fig. 2 and Fig. S1). Additionally, separate images of ab-initio simulations of SAED included in Fig. S2, present the main differences between 2-phases, i.e., ZrO₂-CeO₂, and solid solution ZrO₂/CeO₂ (Fig. S2). The experimental SAED pattern of Au/ZrCe0.05 matches well with the corresponding simulated pattern, and thus confirms the formation of ZrO₂/CeO₂ solid solution. The presence of residual Ce species existing in the form of amorphous CeO₂ is, however, not excluded.

Furthermore, the morphology of Au particles visualized by TEM shows irregular shapes for all the Au particles (Fig. 3). The distribution of Au nanoparticle size is slightly uniform for Au/ZrCe0 catalyst and centered at ca. 35–40 nm, which accounts for 15–17 % of Au particles. In the meantime, a rather broad distribution was recorded for the particle size of Au particles in all the Ce-containing catalysts, which ranges from 10 to 150 nm. Noticeably, at the highest Ce content, Au/ZrCe0.1 catalyst exhibits the highest fraction of Au particles of ca. 70 nm, i.e., 10 %, as

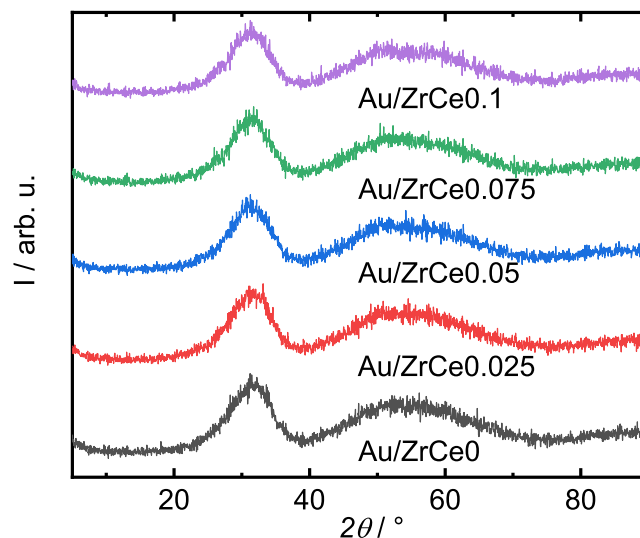


Fig. 1. XRD patterns of the Au/ZrCex catalysts ($x = 0-0.1$).

compared to 0–5 % for other samples (Fig. 3). This indicates that the introduction of Ce using the coprecipitation method did not improve Au dispersion in the amorphous ZrO₂ support materials.

Regarding the textural properties, minor changes were recorded by the N₂ adsorption analyses as displayed in Fig. 4. A Ib-type isotherm with a gradual N₂ uptake over the low relative pressure range ($p/p_0 < 0.4$) was recorded for all the samples suggesting a complex pore structure consisting of wider micropores and narrow mesopores [51]. Further analysis using non-local density functional theory model revealed the pore widths ranging from below 2 nm to 8 nm. Additionally, all the samples exhibit an H2b type hysteresis loop with a gradual delay on desorption branch indicative of a broader neck width distribution compared with the pore width distribution. The values of specific surface area and total pore volume of Au/ZrCex samples are listed in Table 1. The Ce-free catalyst Au/CeZr0, despite the slightly higher N₂ uptake at the relative pressure of 0.6, exhibits a similar porous structure in comparison with the Ce-containing catalysts, ca. $200 \pm 10 \text{ m}^2 \text{ g}^{-1}$ specific surface area (A_{BET}) and ca. $0.13 \pm 0.01 \text{ cm}^3 \text{ g}^{-1}$ total pore volume (V_p).

3.1.2. Redox properties

Concerning the redox properties, the results from H₂-TPR profiles (Fig. 5) provide the very first influence of the introduction of Ce in the Au-based catalyst series. While no signal is visible in the TPR profile of Ce-free catalyst (Au/ZrCe0), the H₂ consumption peak centered in the temperature range of 166–176 °C is recorded for all Ce-containing catalysts. Additional H₂-TPR profiles were recorded for all supports (Fig. S3), in which the peak of interest is absent. The peak is, therefore, associated with the reduction of Au³⁺ to Au⁰ [26,52], which is facilitated in the presence of Ce. This might be explained by the electron redistribution often known for metals supported on CeO₂ due to the formation of surface oxygen vacancies, generated when Ce⁴⁺ cations are reduced to Ce³⁺ rendering to the oxygen transfer process between the metals and CeO₂ support [53]. The interaction between Au and Ce-containing supports gradually increased as suggested by the linear correlation found between the Ce content and the H₂ consumption shown in Table 2. The absence of any reduction peak in Au/ZrCe0 sample is an indication of no positively charged Au in the sample [52,54], and the majority of the Au species is available in the metallic form, which is stable in the oxidation step conducted internally prior to the TPR measurements (see section 2.3). These observations suggest that the Au⁰ formation is more favored in pure ZrO₂ sample, i.e., Au/CeZr0 catalyst, as reported in [54].

Moreover, the synthesized solids were evaluated by XPS to obtain additional information related to the chemical environment of the

Table 1

Elemental content (wAu/Ce/Zr), Ce to Zr molar ratio (n_{Ce}/n_{Zr}), specific surface area (A_{BET}) and total pore volume (V_p) of the Au/ZrCex catalysts ($x = 0-0.1$).

Catalyst	^a wAu wt. %	^a wCe wt. %	^a wZr wt. %	n_{Ce}/n_{Zr}	A_{BET} $\text{m}^2 \text{ g}^{-1}$	V_p $\text{cm}^3 \text{ g}^{-1}$
Au/ZrCe0	0.74	<0.25	58.68	0.00	204	0.14
Au/ZrCe0.025	0.72	1.20	42.57	0.02	196	0.13
Au/ZrCe0.05	0.71	2.46	39.58	0.04	188	0.12
Au/ZrCe0.075	0.71	3.78	35.02	0.07	193	0.12
Au/ZrCe0.1	0.70	4.59	32.48	0.09	197	0.12

^aDetermined by ICP-OES analysis.

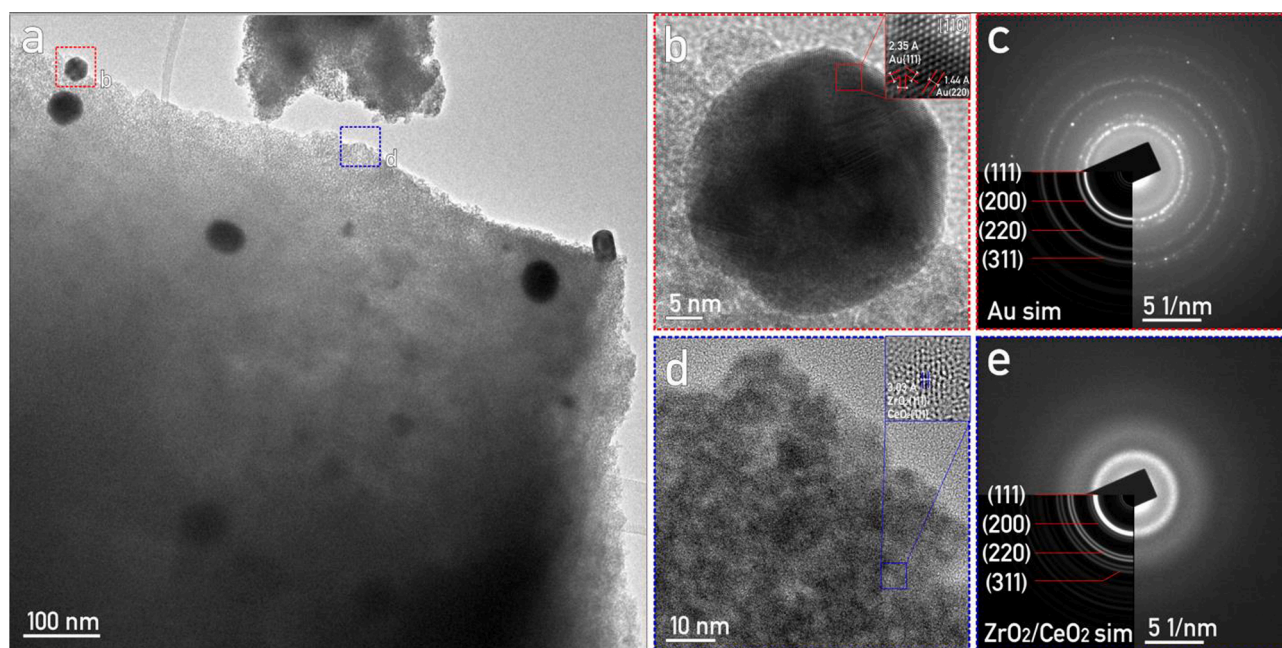


Fig. 2. (a) TEM micrograph of Au/ZrCe0.05 sample with (b) faceted single-crystal nanoparticulates (HR-TEM in $[1-10]$ zone axis, with marked lattice fringe distances in inset), further identified by SAED as (c) pure Au (*ab-initio* simulation in inset). (d) HR-TEM micrograph of the support, with corresponding (e) SAED pattern indicating short-range ordering. In inset is *ab-initio* simulation of electron scattering on the ZrCe solid solution, indexed for ZrO₂.

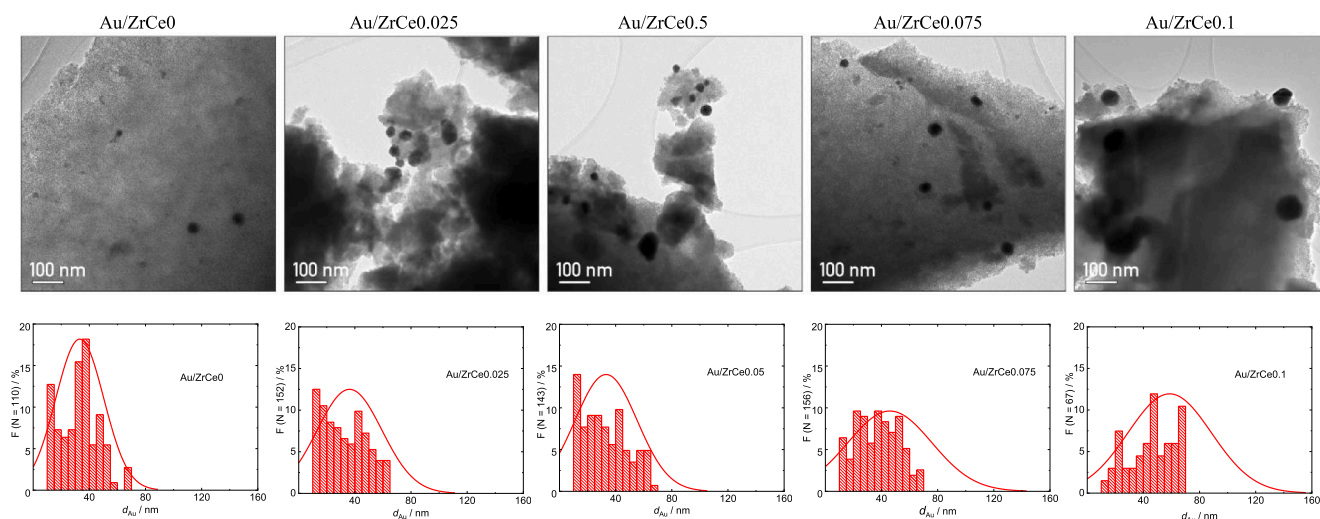


Fig. 3. Overview TEM micrographs of the Au/ZrCex catalysts, with corresponding Au particle size distribution graphs and normal distribution curves.

catalysts. The survey spectra for the surfaces of the samples include O-, Zr-, Au-, and C-containing species indicated by the corresponding signals in Fig. 6. The signal for Ce, i.e., Ce 3d, was detected and thus confirmed the presence of Ce in all the modified samples except for Au/ZrCe0 catalyst.

To investigate the surface chemistry of the synthesized solids in detail, high-resolution XPS spectra were measured and are shown in Fig. 7. The relative quantification of surface Au, Ce and Zr species obtained from XPS is displayed in Table S1.

The surfaces of all samples consisted of C-containing species, i.e. C-C/C-H, C-O, and COO⁻/COOH located at the dashed lines designated in the C 1s spectra (Fig. 7a). These species originate from the adventitious carbonaceous species adsorbed on the surface after sample preparation and transport to the spectrometer. The presence of oxidized carbonaceous species is also confirmed in O 1s spectra, i.e., the spectral feature seen as a shoulder located at dashed line 2 in the O 1s spectra (Fig. 7b).

The main peak at dashed line 1 in the O 1s spectra represents metal oxides. The doublet in the Zr 3d (the Zr 3d_{5/2} main peak at approximately 182 eV) and Au 4f (the Au 4f_{7/2} main peak located at 84.0 eV) spectra correspond to ZrO₂ and Au, respectively. The Zr 3d and Au 4f spectra for all samples tested do not show significant changes in the binding energy (E_B) and the shape of the spectra. This indicates that the Zr and Au environment is similar in all the samples. The observation of similar Au species for all the samples is, however, different from TPR results. The presence of H₂ consumption for all Ce-containing samples, but not the bare ZrO₂, is likely associated with changes in electronic properties induced by the addition of Ce in the ZrO₂ structure.

The spectra of Ce 3d are more complex because they contain many features. It is known that Ce(IV) contains the spectral feature at about 917 eV, which is absent in Ce(III) [55]. The spectra illustrated in Fig. 7e show the feature at approximately 917 eV marked with dashed line in Fig. 7e for all samples except for Au/ZrCe0 catalyst. Therefore, it is

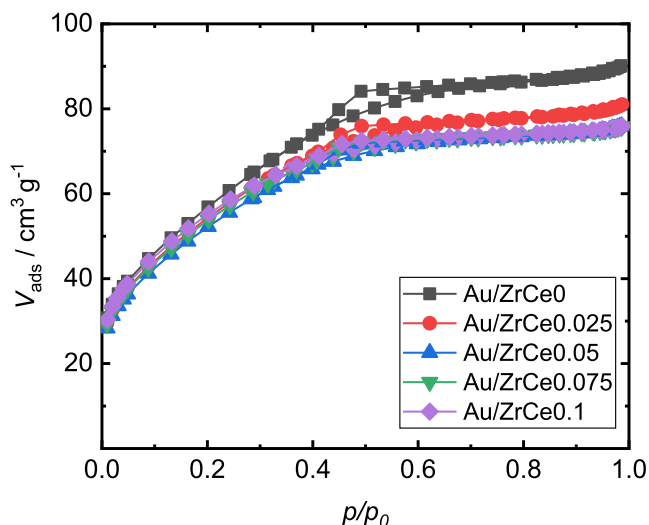


Fig. 4. N_2 sorption isotherms of the Au/ZrCex catalysts ($x = 0-0.1$).

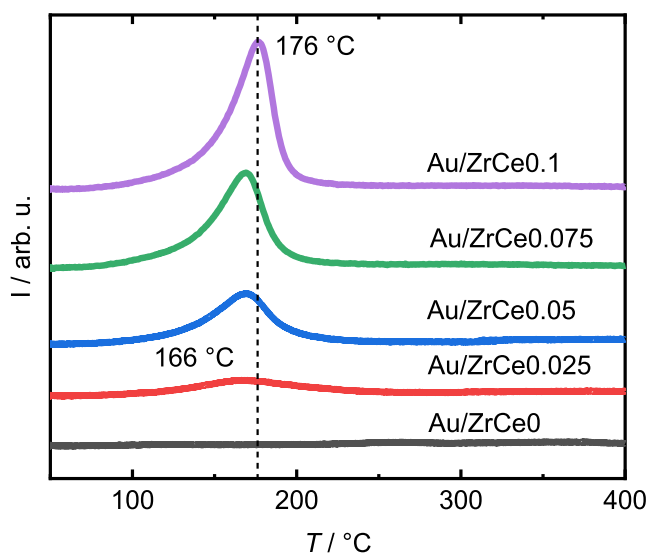


Fig. 5. H_2 -TPR profiles of the Au/ZrCex catalysts ($x = 0-0.1$).

Table 2

H_2 consumption, acid site density (ASD) and base site density (BSD) of the Au/ZrCex catalysts.

Catalyst	H_2 consumption $\mu\text{mol g}^{-1}$	ASD $\mu\text{mol g}^{-1}$	BSD $\mu\text{mol g}^{-1}$
Au/ZrCe0	0	423	99
Au/ZrCe0.025	36	694	210
Au/ZrCe0.05	86	612	143
Au/ZrCe0.075	137	403	98
Au/ZrCe0.1	167	584	120

confirmed that Ce(IV) was present on the surface in all Ce-containing samples. On this basis, the spectra were fitted for the presence of CeO_2 using the positions of the peaks from the previously reported reference spectra [55]. The Ce 3d spectra for CeO_2 consist of two pairs of multiplets (2 pairs of 3 peaks) corresponding to spin-orbit splitting. However, the measured spectra do not fit well with this model probably due to partial reduction of Ce(IV) forming Ce(III) under vacuum conditions (ultra-high vacuum in XPS spectrometer) which is known for CeO_2 [56]. Thus, the spectra of Ce-containing samples were fitted for both Ce(IV) and Ce(III) species (with two doublets [55]). The fitted results match

well with all measured spectra suggesting the presence of these two oxidation states on the surface. The fitted Ce 3d spectrum for the sample Au/CeZr0.1 is exemplarily shown in Fig. 8.

3.1.3. Acidic and basic properties

The basic properties of all Au-containing catalysts were evaluated using CO_2 -TPD analysis and the obtained results are shown in Fig. 9. The CO_2 desorption of Au/ZrCe0 catalyst features a signal centered at ca. 100 °C, and end at ca. 280 °C, which is contributed mainly to the presence of weak basic sites. This peak was also recorded for the Ce-containing catalysts, but it is visible with a considerable broadening and coupled with an additional peak at higher temperatures above 300 °C, which is likely associated with the presence of Ce providing higher basicity than pristine ZrO_2 . However, no clear trend is observed for basic site density (BSD) when the catalysts gradually increases Ce content (Table 2). This suggests that in addition to Ce introduction, the changes in the number of basic sites on the surface of ZrO_2 support are likely affected by other factors, e.g., thermal treatment causing dehydroxylation and formation of acid-base $Zr^{4+}/Ce^{4+}-O^{2-}$ pairs at various extents. Similarly, the influence of Ce introduction on the acid site density (ASD) occurs in a random fashion despite the gradual rise in Ce content as shown in Fig. S4. Interestingly, it was found that the acidic and basic properties of the Au-based catalyst series are closely related, as deduced from a linear regression observed between the acid and basic site density (Table 2). This might be related to the fact that a- ZrO_2 is known to possess mainly coordinatively unsaturated Lewis acid-basic Zr^{4+}/O^{2-} pairs as well as surface hydroxyl groups [57].

3.2. CO_2 hydrogenation activity vs. catalyst properties

The Au-based catalysts supported on ZrO_2 - CeO_2 mixed oxides were tested in the methanol synthesis from CO_2 under various temperatures from 250 to 320 °C as displayed in Table 3. In addition to CO_2 conversion (X_{CO_2}), methanol selectivity (S_{CH_3OH}) and methanol formation rate (r_{CH_3OH}) are employed as measures to evaluate the activity for the methanol synthesis over the Au-based catalysts. Over the studied temperature range, CO_2 conversion varies between 1 % and 11 %, with methanol selectivity up to 27 %, amounting to a methanol formation rate of 1.5 to 4.6 $g_{CH_3OH} \cdot (g_{Au} \cdot h)^{-1}$. Apart from methanol, CO and trace amounts of coke (except for Au/ZrCe0.1 catalyst), no other carbon-containing gas product was found in the discharged gas mixture, and the carbon mass balance is closed up to 85 % to 98 %. The catalytic activity obtained in this study is rather low, in particular, compared with the commercial methanol synthesis. Interestingly, the methanol selectivity of Ce-free Au/ZrCe0 catalyst is significantly lower, i.e., 20 % vs. 72.5 %, in relation to the Au/ ZrO_2 published in a previous work from our group despite the analogous Au content (0.7 wt.% and 0.5 wt.%, respectively) as well as reaction conditions (240–250 °C, 40 bar). This might be explained by the drastic discrepancy in the average Au particle size often reported to play a key role in the hydrogenation activity, i.e., ≈ 40 nm vs. 1.1 nm, respectively. The large size of Au particles might lead to low interfacial Au-support contact and thus facilitates the formation of undesired competitive product CO generated by reverse water gas shift reaction. Moreover, the difference in other properties of the catalysts, e.g., phase composition of ZrO_2 -based support, acidic/basic properties, textural and redox properties, may also play a role.

The reaction temperature, as expected, exhibits a positive effect in the CO_2 conversion independent of Ce content but at the cost of the selectivity to methanol. This agrees well with literature reports [35,58,59] and is attributed to the higher sensitivity to temperature of the CO formation rate in relation to the methanol synthesis, which is evidenced by higher apparent activation energy calculated from Arrhenius plots, e.g., $E_{A,CO} = 64 \text{ kJ mol}^{-1} > E_{A,CH_3OH} = 27 \text{ kJ mol}^{-1}$, as observed in the case of Au/ZrCe0.025 catalyst. The values of E_A for other catalysts are provided in Fig. S5. Besides, all studied catalysts exhibit

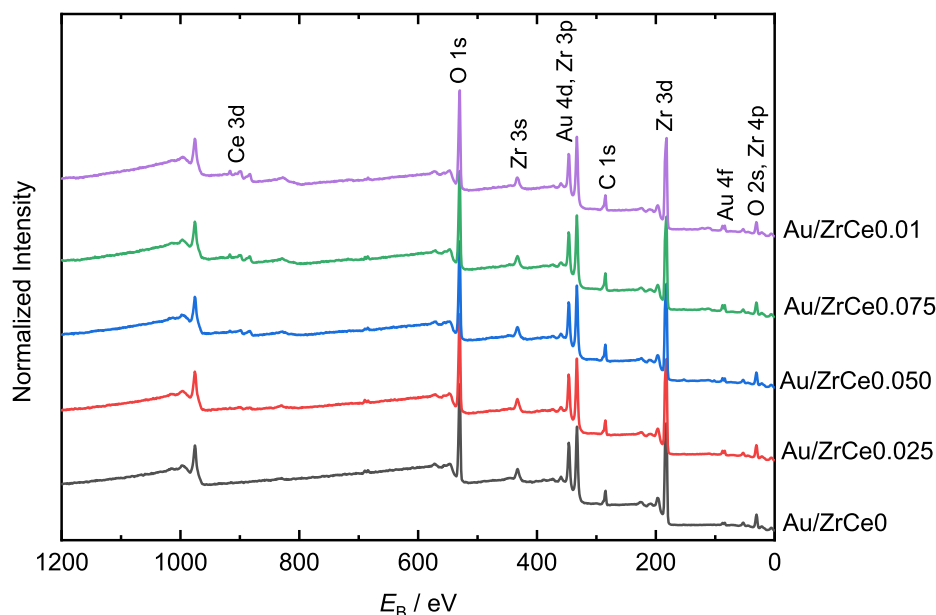


Fig. 6. Survey XPS spectra of the Au/ZrCex catalysts ($x = 0-0.1$).

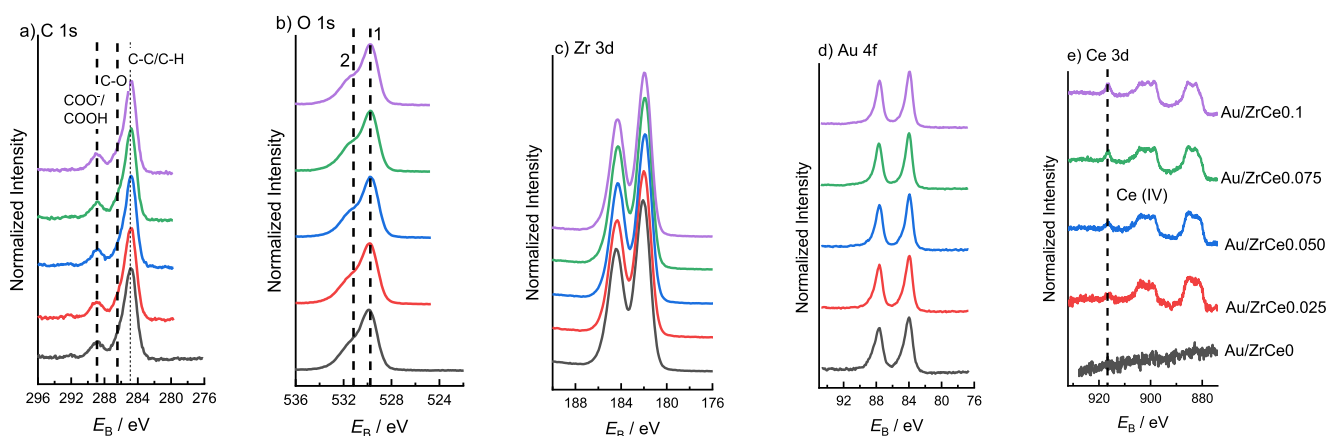


Fig. 7. (a) C 1s, (b) O 1s, (c) Zr 3d, (d) Au 4f, and (e) Ce 3d high-resolution XPS spectra measured for the Au/ZrCex catalysts.

similar apparent activation energy for methanol formation, suggesting that the introduction of Ce did not alter the hydrogenation mechanism of CO_2 into methanol [49]. Consequently, the methanol synthesis via formate intermediate, as proposed in a previous study on Au/a-ZrO₂ catalysts [27], was assumed for the Au-based catalysts in this study. Accordingly, the reaction starts with adsorption and activation of CO_2 and H_2 onto ZrO₂-based support and metallic Au, respectively, which later migrate to the Au-support interface. The dissociated H species react with the activated CO_2 forming mono- and bidentate formates, the two primary intermediates of methanol. Subsequently, the formate species undergo hydrogenation to H_2COO^* , and further terminal protonated to H_2COOH^* , which then cleaves at the C-O bond releasing OH^* and H_2CO^* . The latter participates in hydrogenation, forming H_3CO^* and finally methanol. Among these steps, CO_2 is simultaneously involved in the RWGS process forming undesired product CO.

3.2.1. Ce content and redox properties

Furthermore, while the Ce-free catalyst Au/ZrCe0 exhibits the highest CO_2 conversion (2.3 % at 250 °C) coupled with a 20 % selectivity to methanol, a slightly lower CO_2 conversion was recorded for all the Ce-containing catalysts (Table 3). The decrease in CO_2 conversion is more profound with increasing Ce content. Considering the comparable Au

content as well as the chemical environment of Au, one of the other possible reasons for the decline in CO_2 conversion most likely lies in the large size of Au particles generally accepted to be crucial for its catalytic activity, which was found larger for Ce-containing samples. Besides, catalyst deactivation caused by coke deposition in association with the presence of Ce, as reported by Pojanavaraphan et al. [52], might explain the lower activity in Ce-containing catalysts. However, it is noted that in comparison to the current study, the Ce content was much higher (≥ 25 wt.%) than that presented in this study, and consequently, the negative influence of Ce via boosting carbonaceous species is less likely. In fact, the drop in CO_2 conversion is only considerable for Au/ZrCe0.1 catalyst exhibiting the highest Ce content (4.6 wt.%) and the highest extent of coke deposition (Table 3). On the other hand, the Ce-containing materials, as reported in the literature [25 30,32], exhibit a higher and stronger affinity towards CO_2 molecules, which might lead to active sites poisoning. Additionally, it is worth mentioning that the addition of Ce makes H_2O more favorably adsorbed on the surface [60] and contributes to a blockage of active sites and thus a decline in CO_2 conversion.

Unlike CO_2 conversion, no clear trend was found for methanol selectivity in relation to the presence of Ce. Thus, the next part focuses on the influence of the acidic/basic properties on the methanol selectivity.

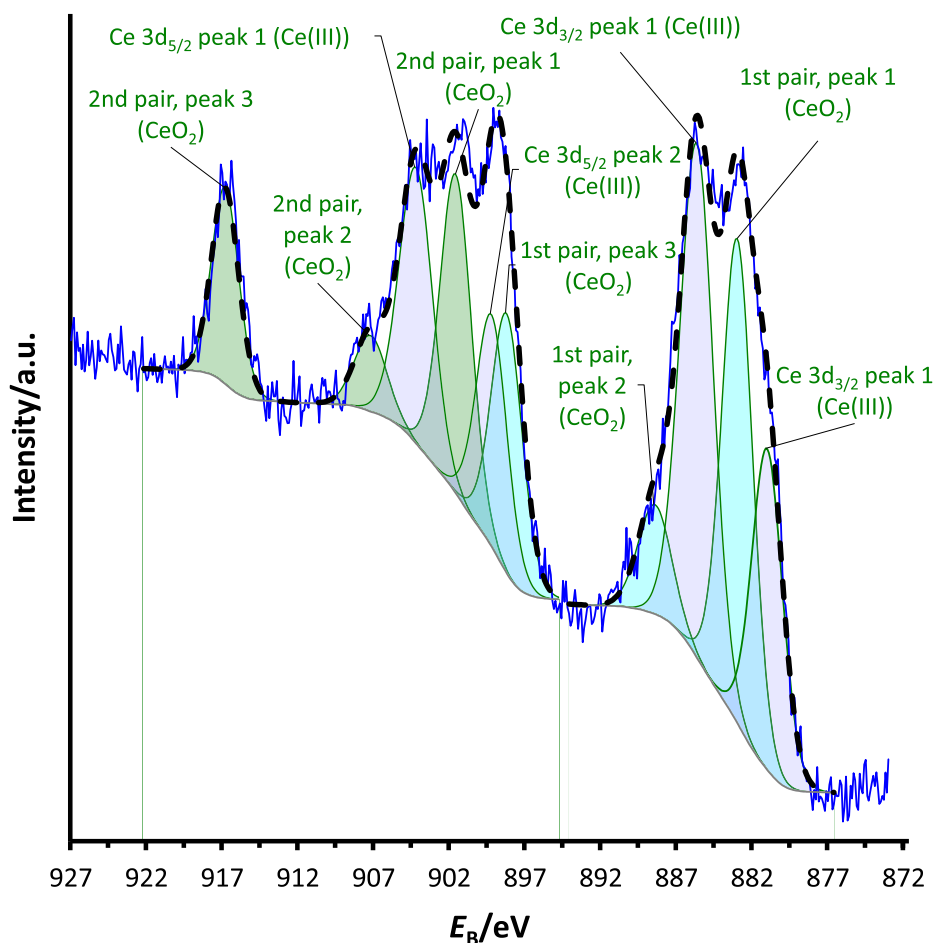


Fig. 8. Ce 3d fitted data for CeO₂ and Ce(III) compounds in Au/CeZr0.1 sample (measured – blue line, fitted – black dashed line).

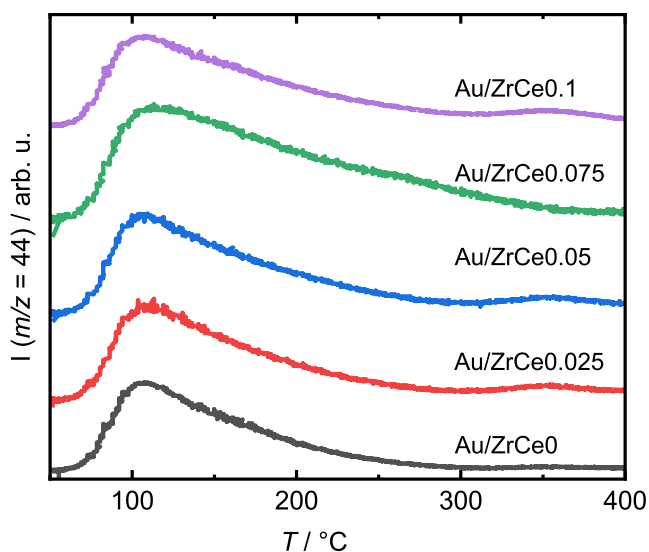


Fig. 9. CO₂-TPD profiles of the Au/ZrCe_x catalysts ($x = 0-0.1$).

3.2.2. Acidic and basic properties

In order to examine relation between methanol selectivity and the catalyst properties, the methanol selectivity S_{CH_3OH} was plotted against the density of base sites (BSD) and acid sites (ASD) as shown in Fig. 10.

Interestingly, volcano-like shaped dependencies were recorded for both BSD and ASD in relation to the methanol selectivity, which

exhibited a critical point of 120 $\mu\text{mol g}^{-1}$ (BSD) and 600 $\mu\text{mol g}^{-1}$ (ASD) at which the highest methanol selectivity of 27 % is reached. The positive effect of the acidity of catalysts in the methanol synthesis was reported in previous studies using Cu/ZrO₂ [55,56]. However, the correlation of the methanol selectivity with gradual changes in acidic/basic properties was not studied. To gain insight into this matter, the nature of acidic and basic sites should be considered. The majority of the acidity and basicity of the investigated catalysts is contributed to the Lewis acid-base pairs, i.e., coordinatively unsaturated Zr⁴⁺-O²⁻, which can reinforce the adsorption of CO₂, particularly, the interaction between O and C atoms of CO₂ molecules with Zr⁴⁺ and O²⁻, respectively [49]. Moreover, in the presence of Ce, the adsorption of CO₂ forming monodentate carbonates, which was not observed for pristine ZrO₂, is facilitated as suggested by density functional theory (DFT) results obtained for t-ZrO₂ incorporated with ca. 2 wt.% Ce [60]. Monodentate carbonate is an important precursor to the more stable bidentate carbonate, which can be further converted into bidentate formate and subsequently to methanol via the formate reaction pathway. Besides, these Lewis acid-base pairs can also participate in the dissociation of water molecules generating surface hydroxyl groups, which can promote methanol synthesis via reacting with carbonate species, forming mono-/bidentate formates [61]. The eased formation of formates might hinder the competitive process, RWGS, as suggested by various studies [34,62], and thus increase the methanol selectivity. Alternatively, the methanol synthesis can also be facilitated via the hydrogenation of CO [57], which is, however, unlikely in this study as the CO adsorption was suggested to be hardly affected by Ce incorporation at low content [60]. Thus, the increase of the acid-base pairs in numbers, as well as strength, probably renders to the improved methanol selectivity (Fig. 10).

Table 3

CO₂ conversion (X_{CO_2}), selectivity to methanol (S_{CH_3OH}) and CO (S_{CO}), methanol formation rate (r_{CH_3OH}) and C content (wC) of fresh and spent Au/CeZrx catalysts after the hydrogenation of CO₂ at various reaction temperature (250–320 °C).

Catalyst	T °C	X_{CO_2} %	S_{CH_3OH} %	S_{CO} %	$r_{CH_3OH} S_{CH_3OH} \bullet (g_{Au} \bullet h)^{-1}$	^a wC wt.%	
						fresh	spent
Au/ZrCe0	250	2.3	20	78	2.03	0.5	0.6
	280	4.6	15	85	3.05		
	300	6.9	12	80	3.69		
	320	9.9	9	78	4.01		
Au/ZrCe0.025	250	2.1	22	61	2.09	0.6	0.8 ^b 0.7
	280	3.6	21	63	3.36		
	300	6.2	14	78	4.01		
	320	8.9	11	79	4.29		
Au/ZrCe0.05	250	1.7	26	72	1.95	0.6	0.8
	280	3.8	20	83	3.35		
	300	6.9	13	78	4.21		
	320	11.2	9	70	4.63		
Au/ZrCe0.075	250	1.5	22	60	1.50	0.6	0.8
	280	3.6	15	63	2.49		
	300	5.1	14	78	3.22		
	320	8.7	9	70	3.66		
Au/ZrCe0.1	250	1.4	27	53	1.79	0.6	1.1
	280	3.3	18	67	2.77		
	300	4.6	16	77	3.36		
	320	8.0	10	71	3.91		

Reaction conditions: $m_{cat.} = 200$ mg, $Q_{CO_2+H_2} = 40$ mL min⁻¹, $H_2/CO_2 = 3:1$ (v/v), 40 bar.

^aDetermined by means of CHNS elemental analysis.

^bAfter 93 h.

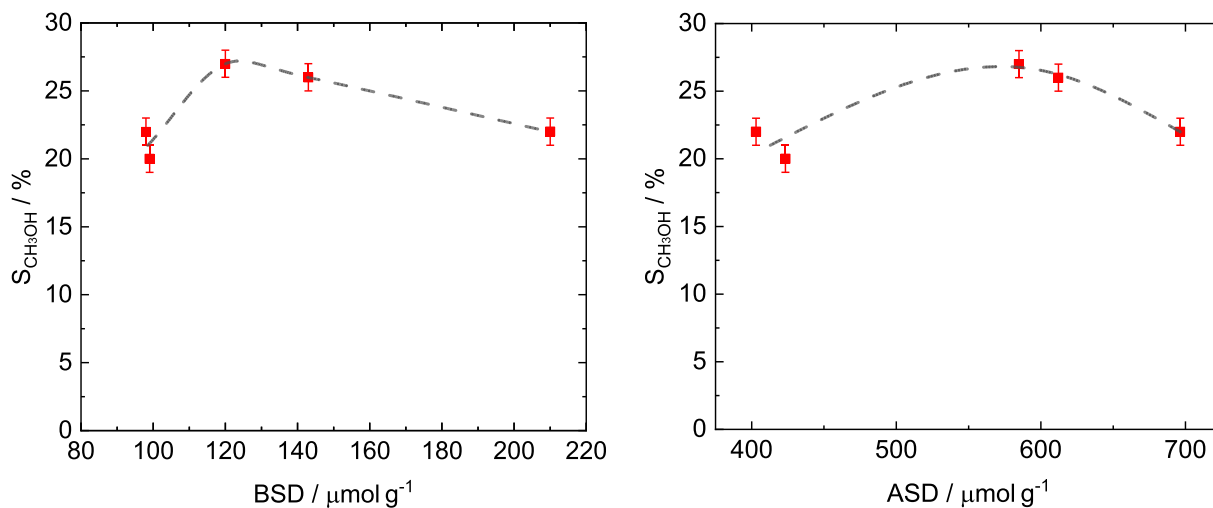


Fig. 10. Methanol selectivity (■) as a function of base site density (BSD, left) and acid site density (ASD, right) in the hydrogenation of CO₂ over the Au/ZrCex catalysts ($x = 0-0.1$). The dash lines highlight trends. Reaction conditions: $m_{cat.} = 200$ mg, $Q_{CO_2+H_2} = 40$ mL min⁻¹, $H_2/CO_2 = 3:1$ (v/v), 40 bar, 250 °C.

Nevertheless, the interface between the multiple components of the catalysts, i.e., metallic sites, hydroxyl groups and the acid-base pairs, seemingly plays a crucial role in the methanol synthesis as depicted in Fig. 11, which might explain the decrease in methanol selectivity when further increasing the number of acid/basic sites. The surface catalytic sites probably suffer catalyst deactivation due to blockage of active sites by a multilayer of adsorbed CO₂ or intermediates.

3.3. Catalytic stability of Au/ZrCe catalysts in the CO₂ hydrogenation

Considering the highest methanol formation rate among the Ce-containing Au-based catalysts, Au/ZrCe0.025 sample was selectively investigated in the catalytic stability carried out throughout 93 h under reaction conditions (280 °C and 40 bar) (Fig. 12). The obtained results suggest a stable performance through the whole experiment with a CO₂ conversion of 3.5 ± 0.2 % rendering to a methanol formation rate of 3.32 ± 0.25 g_{CH₃OH} • (g_{Au} • h)⁻¹. Noticeably, with respect to the start of

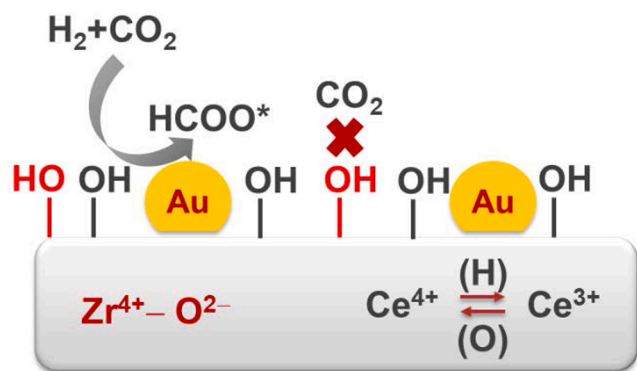


Fig. 11. Proposed scheme explaining the influence of the Au/ZrCe catalysts in the hydrogenation of CO₂.

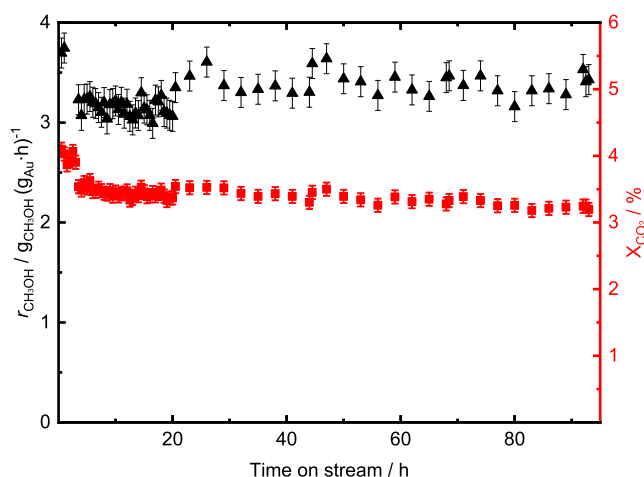


Fig. 12. Methanol formation rate (▲) and CO₂ conversion (■) as a function of time on stream (TOS) in the CO₂ hydrogenation over Au/ZrCe0.025 catalyst. Reaction conditions: $m_{\text{cat.}} = 200$ mg, $Q_{\text{CO}_2+\text{H}_2} = 40$ mL min⁻¹, H₂/CO₂ = 3:1 (v/v), 40 bar, 280 °C, 93 h.

the experiment, there is a slight loss of catalytic activity by 0.6 % in CO₂ conversion and 0.47 $g_{\text{CH}_3\text{OH}} \cdot (g_{\text{Au}} \cdot \text{h})^{-1}$ in ($r_{\text{CH}_3\text{OH}}$) occurring in the first 3 h, which might be due to the considerable formation of water via RWGS causing saturation of the support surface due to high affinity to water in the presence of Ce [60]. Nevertheless, the reactivity of the catalyst (Au/ZrCe0.025) was steady for the next 90 h. Despite the long reaction time, the coke deposition is negligible as deduced from the marginal discrepancy in the consumed catalyst's C content, i.e., 0.7 wt.% (spent) vs. 0.6 wt.% (fresh).

4. Conclusions

In summary, this study presents a systematic investigation of the influence of Ce in the Au catalysts supported on amorphous ZrO₂ prepared via the simple coprecipitation method. The newly introduced Ce was present in the form of both Ce(III) and Ce(IV), which does not alter the textural properties compared to the pristine ZrO₂ materials with a Ce content up to 4.6 wt.%. The Ce-containing catalysts show a slightly lower Au dispersion evidenced by large particles (ca. 40 nm) and a broad distribution ranging from 5 to 125 nm. Besides, the formation of metallic Au is less favored and coupled with increased Au cations with rising Ce content, probably due to the electron exchange between Au and CeO₂. These findings might explain the decrease of CO₂ conversion with increasing Ce content of Au catalysts supported on ZrO₂-CeO₂ mixed oxides in the hydrogenation of CO₂. In addition to methanol formed via

formate intermediates, only CO was observed as a side product under the studied reaction conditions (typically at 40 bar and 250–320 °C), irrespectively of the catalysts employed. It was proven that acid-base properties play a role in CO₂ adsorption/activation and thus in tailoring the product distribution of the CO₂ hydrogenation. The selectivity of the desired product methanol was found to be closely associated with the number of both acidic and basic sites of the catalysts in a volcano-shape fashion. In particular, there is a critical point of acid/base site density, at which the methanol selectivity reaches a maximum 27 % (at 40 bar and 280 °C), which is 120 and 600 $\mu\text{mol g}^{-1}$, respectively. The Au catalysts on CeO₂-ZrO₂ mixed oxides exhibit excellent catalytic stability, for example, the methanol formation rate of 3.32 $g_{\text{CH}_3\text{OH}} \cdot (g_{\text{Au}} \cdot \text{h})^{-1}$ recorded for Au/ZrCe0.025 catalyst at 250 °C and 40 bar remained for up to 93 h TOS.

CRediT authorship contribution statement

Hue-Tong Vu: Investigation, Methodology, Visualization, Writing – original draft, Writing – review & editing. **Matjaž Finšgar:** Funding acquisition, Investigation, Writing – review & editing. **Janez Zavašnik:** Investigation, Writing – review & editing. **Nataša Novak Tušar:** Funding acquisition, Supervision, Writing – review & editing. **Albin Pintar:** Funding acquisition, Project administration, Conceptualization, Supervision, Visualization, Writing – review & editing.

Declaration of Competing Interest

The authors declare that they have no known competing financial interests or personal relationships that could have appeared to influence the work reported in this paper.

Data availability

Data will be made available on request.

Acknowledgements

This research was funded by the Slovenian Research Agency, grant numbers J7-3151, P1-0418 and P2-0118. The project is co-financed by the Republic of Slovenia, the Ministry of Education, Science and Sport and the European Union under the European Regional Development Fund. The authors thank Mojca Opresnik, Edi Kranjc, Špela Božič, Iris Štucin, Matevž Roškarič, and Gregor Žerjav from the National Institute of Chemistry (Ljubljana, Slovenia) for N₂ sorption, XRD, CHN, ICP-OES analyses and their support in the labs, respectively. Janez Zavašnik acknowledges the support via ARRS P1-0417.

Appendix A. Supplementary data

Supplementary data to this article can be found online at <https://doi.org/10.1016/j.apsusc.2023.156737>.

References

- [1] X. Jiang, X. Nie, X. Guo, C. Song, J.G. Chen, Recent Advances in Carbon Dioxide Hydrogenation to Methanol via Heterogeneous Catalysis, Chem. Rev. 120 (2020) 7984–8034, <https://doi.org/10.1021/acs.chemrev.9b00723>.
- [2] T. Numpilai, P. Kidkhunthod, C.K. Cheng, C. Wattanakit, M. Chareonpanich, J. Limtrakul, T. Wittoon, CO₂ hydrogenation to methanol at high reaction temperatures over In₂O₃/ZrO₂ catalysts: Influence of calcination temperatures of ZrO₂ support, Catal. Today. 375 (2021) 298–306, <https://doi.org/10.1016/j.cattod.2020.03.011>.
- [3] F. Zeng, C. Mebrahtu, X. Xi, L. Liao, J. Ren, J. Xie, H.J. Heeres, R. Palkovits, Catalysts design for higher alcohols synthesis by CO₂ hydrogenation: Trends and future perspectives, Appl. Catal. B 291 (2021), 120073, <https://doi.org/10.1016/j.apcatb.2021.120073>.
- [4] T. Wittoon, T. Numpilai, S. Nijpanich, N. Chanlek, P. Kidkhunthod, C.K. Cheng, K. H. Ng, D.-V.-N. Vo, S. Ittisanronnachai, C. Wattanakit, M. Chareonpanich, J. Limtrakul, Enhanced CO₂ hydrogenation to higher alcohols over K-Co promoted

- In₂O₃ catalysts, *Chem. Eng. J.* 431 (2022), 133211, <https://doi.org/10.1016/j.cej.2021.133211>.
- [5] T.T.N. Vu, A. Desgagnés, M.C. Iliuta, Efficient approaches to overcome challenges in material development for conventional and intensified CO₂ catalytic hydrogenation to CO, methanol, and DME, *Appl. Catal. A. Gen.* 617 (2021), 118119, <https://doi.org/10.1016/j.apcata.2021.118119>.
- [6] L. Guo, J. Sun, Q. Ge, N. Tsubaki, Recent advances in direct catalytic hydrogenation of carbon dioxide to valuable C₂₊ hydrocarbons, *J. Mater. Chem. A: Mater. Energy Sustainability* 6 (2018) 23244–23262, <https://doi.org/10.1039/C8TA05377D>.
- [7] B. Pawelec, R. Guil-López, N. Mota, J.L.G. Fierro, R.M. Navarro Yerga, Catalysts for the conversion of CO₂ to low molecular weight olefins—a review, *Materials* 14 (2021) 6952, <https://doi.org/10.3390/ma14226952>.
- [8] T. Witton, V. Lapkeatsere, T. Numpilai, C. Kui Cheng, J. Limtrakul, CO₂ hydrogenation to light olefins over mixed Fe-Co-K-Al oxides catalysts prepared via precipitation and reduction methods, *Chem. Eng. J.* 428 (2022), 131389, <https://doi.org/10.1016/j.cej.2021.131389>.
- [9] H. Kim, M. Byun, B. Lee, H. Lim, Carbon-neutral methanol synthesis as carbon dioxide utilization at different scales: Economic and environmental perspectives, *Energy Convers. Manag.* 252 (2022), 115119, <https://doi.org/10.1016/j.enconman.2021.115119>.
- [10] S. Poto, D. Vico van Berkel, F. Gallucci, M. Fernanda Neira d'Angelo, Kinetic modelling of the methanol synthesis from CO₂ and H₂ over a CuO/CeO₂/ZrO₂ catalyst: The role of CO₂ and CO hydrogenation, *Chem. Eng. J.* 435 (2022) 134946, <https://doi.org/10.1016/J.CEJ.2022.134946>.
- [11] L.A. Curtiss, K. Raghavachari, P.C. Redfern, J.A. Pople, Assessment of Gaussian-2 and density functional theories for the computation of enthalpies of formation, *J. Chem. Phys.* 106 (1998) 1063, <https://doi.org/10.1063/1.473182>.
- [12] S. Kanuri, S. Roy, C. Chakraborty, S. Prasad Datta, S.A. Singh, S. Dinda, C. A. Satyapaul Singh, An insight of CO₂ hydrogenation to methanol synthesis: Thermodynamics, catalysts, operating parameters, and reaction mechanism, *Int. J. Energy Res.* (2021) 1–20, <https://doi.org/10.1002/ER.7562>.
- [13] C. Temvutitirojn, Y. Poo-Arporn, N. Chanlek, C.K. Cheng, C.C. Chong, J. Limtrakul, T. Witton, Role of Calcination Temperatures of ZrO₂ Support on Methanol Synthesis from CO₂ Hydrogenation at High Reaction Temperatures over ZnO_x/ZrO₂ Catalysts, *Ind. Eng. Chem. Res.* 59 (2020) 5525–5535, https://doi.org/10.1021/ACS.IECR.9B05691/ASSET/IMAGES/MEDIUM/IE9B05691_0014.GIF.
- [14] S.T. Bai, G. de Smet, Y. Liao, R. Sun, C. Zhou, M. Beller, B.U.W. Maes, B.F. Sels, Homogeneous and heterogeneous catalysts for hydrogenation of CO₂ to methanol under mild conditions, *Chem. Soc. Rev.* 50 (2021) 4259–4298, <https://doi.org/10.1039/d0cs01331e>.
- [15] E. Kondratenko, G. Mul, J. Baltrusaitis, G.O. Larrazábal, J. Pérez-Ramírez, Status and perspectives of CO₂ conversion into fuels and chemicals by catalytic, photocatalytic and electrocatalytic processes, *Energy Environ. Sci.* 6 (2013) 3112, <https://doi.org/10.1039/c3ee41272e>.
- [16] G. Zhao, X. Huang, X. Wang, X. Wang, Progress in catalyst exploration for heterogeneous CO₂ reduction and utilization: a critical review, *J. Mater. Chem. A: Mater. Energy Sustainability* 5 (2017) 21625–21649, <https://doi.org/10.1039/C7TA07290B>.
- [17] Q. Wu, S. Liang, T. Zhang, B. Louis, Q. Wang, Current advances in bimetallic catalysts for carbon dioxide hydrogenation to methanol, *Fuel* 313 (2022), 122963, <https://doi.org/10.1016/J.FUEL.2021.122963>.
- [18] J.W.M. Crawley, I.E. Gow, N. Lawes, I. Kowalec, L. Kabanal, C.R.A. Catlow, A. J. Logsdail, S.H. Taylor, N.F. Dummer, G.J. Hutchings, Heterogeneous Trimetallic Nanoparticles as Catalysts, *Chem. Rev.* 122 (2022) 6795–6849, <https://doi.org/10.1021/ACS.CHEMREV.1C00493>.
- [19] M. Zabilskiy, K. Ma, A. Beck, J.A. van Bokhoven, Methanol synthesis over Cu/CeO₂-ZrO₂ catalysts: The key role of multiple active components, *Catal. Sci. Technol.* 11 (2021) 349–358, <https://doi.org/10.1039/d0cy01762k>.
- [20] W.J. Shen, Y. Ichihashi, Y. Matsumura, Low temperature methanol synthesis from carbon monoxide and hydrogen over ceria supported copper catalyst, *Appl. Catal. A. Gen.* 282 (2005) 221–226, <https://doi.org/10.1016/J.APCATA.2004.12.046>.
- [21] V.D.B.C. Dasireddy, B. Likozar, The role of copper oxidation state in Cu/ZnO/Al₂O₃ catalysts in CO₂ hydrogenation and methanol productivity, *Renew. Energy* 140 (2019) 452–460, <https://doi.org/10.1016/J.RENENE.2019.03.073>.
- [22] Y. Wang, S. Kattel, W. Gao, K. Li, P. Liu, J.G. Chen, H. Wang, Exploring the ternary interactions in Cu–ZnO–ZrO₂ catalysts for efficient CO₂ hydrogenation to methanol, *Nature Communications* 2019 10:1. 10 (2019) 1–10, <https://doi.org/10.1038/s41467-019-09072-6>.
- [23] T. Witton, J. Chalorntham, P. Dumrongbunditkul, M. Chareonpanich, J. Limtrakul, CO₂ hydrogenation to methanol over Cu/ZrO₂ catalysts: Effects of zirconia phases, *Chem. Eng. J.* 293 (2016) 327–336, <https://doi.org/10.1016/j.cej.2016.02.069>.
- [24] M. Haruta, When Gold Is Not Noble: Catalysis by Nanoparticles, *The Chemical Record* 3 (2003) 75–87, <https://doi.org/10.1002/TCR.10053>.
- [25] Y. Hartadi, D. Widmann, R.J. Behm, CO₂ hydrogenation to methanol on supported Au catalysts under moderate reaction conditions: Support and particle size effects, *ChemSusChem* 8 (2015) 456–465, <https://doi.org/10.1002/CS5C.201402645>.
- [26] J. Wang, H. Tan, S. Yu, K. Zhou, Morphological effects of gold clusters on the reactivity of ceria surface oxygen, *ACS Catal.* 5 (2015) 2873–2881, https://doi.org/10.1021/CS502055R/SUPPL_FILE/CS502055R_SI_001.PDF.
- [27] T.V. Sagar, J. Zavašnik, M. Finšgar, N. Novak Tušar, A. Pintar, Evaluation of Au/ZrO₂ Catalysts Prepared via Postsynthesis Methods in CO₂ Hydrogenation to Methanol, *Catalysts* 12 (2022) 218, <https://doi.org/10.3390/catal12020218>.
- [28] A. Baiker, M. Kilo, M. Maciejewski, S. Menzi, A. Wokaun, Hydrogenation of CO₂ Over Copper, Silver and Gold/Zirconia Catalysts: Comparative Study of Catalyst Properties and Reaction Pathways, *Stud. Surf. Sci. Catal.* 75 (1993) 1257–1272, [https://doi.org/10.1016/S0167-2991\(08\)64449-3](https://doi.org/10.1016/S0167-2991(08)64449-3).
- [29] S. Kattel, P. Liu, J.G. Chen, Tuning Selectivity of CO₂ Hydrogenation Reactions at the Metal/Oxide Interface, *J. Am. Chem. Soc.* 139 (2017) 9739–9754, <https://doi.org/10.1021/JACS.7B05362>.
- [30] H. Sakurai, M. Haruta, Carbon dioxide and carbon monoxide hydrogenation over gold supported on titanium, iron, and zinc oxides, *Appl. Catal. A. Gen.* 127 (1995) 93–105, [https://doi.org/10.1016/0926-860X\(95\)00058-5](https://doi.org/10.1016/0926-860X(95)00058-5).
- [31] H. Sakurai, M. Haruta, Synergism in methanol synthesis from carbon dioxide over gold catalysts supported on metal oxides, *Catal. Today* 29 (1996) 361–365, [https://doi.org/10.1016/0920-5861\(95\)00305-3](https://doi.org/10.1016/0920-5861(95)00305-3).
- [32] H. Sakurai, S. Tsubota, M. Haruta, Hydrogenation of CO₂ over gold supported on metal oxides, *Appl. Catal. A. Gen.* 102 (1993) 125–136, [https://doi.org/10.1016/0926-860X\(93\)80224-E](https://doi.org/10.1016/0926-860X(93)80224-E).
- [33] W. Wang, Z. Qu, L. Song, Q. Fu, CO₂ hydrogenation to methanol over Cu/CeO₂ and Cu/ZrO₂ catalysts: Tuning methanol selectivity via metal-support interaction, *J. Energy Chem.* 40 (2020) 22–30, <https://doi.org/10.1016/J.JEICHEM.2019.03.001>.
- [34] J. Zhu, Y. Su, J. Chai, V. Muravev, N. Kosinov, E.J.M. Hensen, Mechanism and Nature of Active Sites for Methanol Synthesis from CO/CO₂ on Cu/CeO₂, *ACS Catal.* 10 (2020) 11532–11544, <https://doi.org/10.1021/acscatal.0c02909>.
- [35] W. Wang, Z. Qu, L. Song, Q. Fu, An investigation of Zr/Ce ratio influencing the catalytic performance of CuO/Ce_{1-x}Zr_xO₂ catalyst for CO₂ hydrogenation to CH₃OH, *J. Energy Chem.* 47 (2020) 18–28, <https://doi.org/10.1016/j.jechem.2019.11.021>.
- [36] K. Chang, H. Zhang, M.J. Cheng, Q. Lu, Application of Ceria in CO₂ Conversion Catalysis, *ACS Catal.* 10 (2020) 613–631, <https://doi.org/10.1021/acscatal.9b03935>.
- [37] F. Wang, M. Wei, D.G. Evans, X. Duan, CeO₂-based heterogeneous catalysts toward catalytic conversion of CO₂, *J. Mater. Chem. A: Mater. Energy Sustainability* 4 (2016) 5773–5783, <https://doi.org/10.1039/C5TA10737G>.
- [38] L.F. Rasteiro, R.A. de Sousa, L.H. Vieira, V.K. Ocampo-Restrepo, L.G. Verga, J. M. Assaf, J.L.F. da Silva, E.M. Assaf, Insights into the alloy-support synergistic effects for the CO₂ hydrogenation towards methanol on oxide-supported Ni₅Ga₃ catalysts: An experimental and DFT study, *Appl. Catal. B* 302 (2022), 120842, <https://doi.org/10.1016/j.apcatb.2021.120842>.
- [39] X. Yang, S. Kattel, S.D. Senanayake, J.A. Boscoboinik, X. Nie, J. Graciani, J. A. Rodriguez, P. Liu, D.J. Stacchiola, J.G. Chen, Low pressure CO₂ hydrogenation to methanol over gold nanoparticles activated on a CeO_x/TiO₂ Interface, *J. Am. Chem. Soc.* 137 (2015) 10104–10107, <https://doi.org/10.1021/jacs.5b06150>.
- [40] A. Jangam, P. Hongmanorom, M.H. Wai, A.J. Poerjoto, S. Xi, A. Borgna, S. Kawi, CO₂ Hydrogenation to Methanol over Partially Reduced Cu-SiO_{2p} Catalysts: The Crucial Role of Hydroxyls for Methanol Selectivity, *ACS Appl. Energy Mater.* 4 (2021) 12149–12162, <https://doi.org/10.1021/acsaem.1c01734>.
- [41] Y. Peng, L. Wang, Q. Luo, Y. Cao, Y. Dai, Z. Li, H. Li, X. Zheng, W. Yan, J. Yang, J. Zeng, Molecular-Level Insight into How Hydroxyl Groups Boost Catalytic Activity in CO₂ Hydrogenation into Methanol, *Chem.* 4 (2018) 613–625, <https://doi.org/10.1016/J.CHEMPR.2018.01.019>.
- [42] C. Yang, R. Mu, G. Wang, J. Song, H. Tian, Z.J. Zhao, J. Gong, Hydroxyl-mediated ethanol selectivity of CO₂ hydrogenation, *Chem. Sci.* 10 (2019) 3161–3167, <https://doi.org/10.1039/C8SC05608K>.
- [43] R. Zhang, B. Wang, H. Liu, L. Ling, Effect of surface hydroxyls on CO₂ hydrogenation over Cu/γ-Al₂O₃ catalyst: A theoretical study, *J. Phys. Chem. C* 115 (2011) 19811–19818, https://doi.org/10.1021/JP206065Y/SUPPL_FILE/JP206065Y_SI_001.PDF.
- [44] R. Khobragade, M. Roškaric, G. Žerjav, M. Košiček, J. Zavašnik, N. van de Velde, I. Jerman, N.N. Tušar, A. Pintar, Exploring the effect of morphology and surface properties of nanoshaped Pd/CeO₂ catalysts on CO₂ hydrogenation to methanol, *Appl. Catal. A. Gen.* 627 (2021), 118394, <https://doi.org/10.1016/j.apcata.2021.118394>.
- [45] F. Jiang, S. Wang, B. Liu, J. Liu, L. Wang, Y. Xiao, Y. Xu, X. Liu, Insights into the Influence of CeO₂ Crystal Facet on CO₂ Hydrogenation to Methanol over Pd/CeO₂ Catalysts, *ACS Catal.* 10 (2020) 11493–11509, <https://doi.org/10.1021/acscatal.0c03324>.
- [46] F. Xie, S. Xu, L. Deng, H. Xie, G. Zhou, CO₂ hydrogenation on Co/CeO_{2-s} catalyst: Morphology effect from CeO₂ support, *Int. J. Hydrogen Energy* 45 (2020) 26938–26952, <https://doi.org/10.1016/j.ijhydene.2020.05.260>.
- [47] M.K. Koh, M. Khavarian, S.P. Chai, A.R. Mohamed, The morphological impact of siliceous porous carriers on copper-catalysts for selective direct CO₂ hydrogenation to methanol, *Int. J. Hydrogen Energy* 43 (2018) 9334–9342, <https://doi.org/10.1016/J.IJHYDENE.2018.03.202>.
- [48] M. Konsolakis, M. Lykaki, S. Stefa, S.A.C. Carabineiro, G. Varvoutis, E. Pajista, G. E. Marnellos, CO₂ hydrogenation over nanoceria-supported transition metal catalysts: Role of ceria morphology (nanorods versus nanocubes) and active phase nature (Co versus Cu), *Nanomaterials* 9 (2019) 1739, <https://doi.org/10.3390/nano9121739>.
- [49] B. Bachiller-Baeza, I. Rodriguez-Ramos, A. Guerrero-Ruiz, Interaction of Carbon Dioxide with the Surface of Zirconia Polymorphs, *Langmuir* 14 (1998) 3556–3564, <https://doi.org/10.1021/la970856q>.
- [50] D.A. Shirley, High-Resolution X-Ray Photoemission Spectrum of the Valence Bands of Gold, *Phys. Rev. B* 5 (1972) 4709, <https://doi.org/10.1103/PhysRevB.5.4709>.
- [51] K.A. Cychosz, R. Guillet-Nicolas, J. García-Martínez, M. Thommes, Recent advances in the textural characterization of hierarchically structured nanoporous materials, *Chem. Soc. Rev.* 46 (2017) 389–414, <https://doi.org/10.1039/C6CS00391E>.

- [52] C. Pojanavaraphan, W. Nakaranuwattana, A. Luengnaruemitchai, E. Gulari, Effect of support composition and metal loading on Au/Ce_{1-x}Zr_xO₂ catalysts for the oxidative steam reforming of methanol, *Chem. Eng. J.* 240 (2014) 99–108, <https://doi.org/10.1016/J.CEJ.2013.11.062>.
- [53] A. Ruiz, P. Schlexer, S. Tosoni, G. Pacchioni, Increasing Oxide Reducibility: The Role of Metal/Oxide Interfaces in the Formation of Oxygen Vacancies, *ACS Catal.* 7 (2017) 6493–6513, <https://doi.org/10.1021/acscatal.7b01913>.
- [54] A. Vourros, I. Garagounis, V. Kyriakou, S.A.C. Carabineiro, F.J. Maldonado-Hódar, G.E. Marnellos, M. Konsolakis, Carbon dioxide hydrogenation over supported Au nanoparticles: Effect of the support, *J. CO₂ Util.* 19 (2017) 247–256, <https://doi.org/10.1016/J.JCOU.2017.04.005>.
- [55] E. Bèche, P. Charvin, D. Perarnau, S. Abanades, G. Flamant, Ce 3d XPS investigation of cerium oxides and mixed cerium oxide (Ce_xTi_yO₂), *Surf. Interface Anal.* 40 (2008) 264–267, <https://doi.org/10.1002/sia.2686>.
- [56] F. Zhang, P. Wang, J. Koberstein, S. Khalid, S.W. Chan, Cerium oxidation state in ceria nanoparticles studied with X-ray photoelectron spectroscopy and absorption near edge spectroscopy, *Surf. Sci.* 563 (2004) 74–82, <https://doi.org/10.1016/J.SUSC.2004.05.138>.
- [57] Z.Y. Ma, C. Yang, W. Wei, W.H. Li, Y.H. Sun, Surface properties and CO adsorption on zirconia polymorphs, *J. Mol. Catal. A Chem.* 227 (2005) 119–124, <https://doi.org/10.1016/J.MOLCATA.2004.10.017>.
- [58] C.Y. Regalado Vera, N. Manavi, Z. Zhou, L.C. Wang, W. Diao, S. Karakalos, B. Liu, K.J. Stowers, M. Zhou, H. Luo, D. Ding, Mechanistic understanding of support effect on the activity and selectivity of indium oxide catalysts for CO₂ hydrogenation, *Chem. Eng. J.* 426 (2021), 131767, <https://doi.org/10.1016/J.CEJ.2021.131767>.
- [59] F.C.F. Marcos, F.M. Cavalcanti, D.D. Petrolini, L. Lin, L.E. Betancourt, S. D. Senanayake, J.A. Rodriguez, J.M. Assaf, R. Giudici, E.M. Assaf, Effect of operating parameters on H₂/CO₂ conversion to methanol over Cu-Zn oxide supported on ZrO₂ polymorph catalysts: Characterization and kinetics, *Chem. Eng. J.* 427 (2022), 130947, <https://doi.org/10.1016/J.CEJ.2021.130947>.
- [60] F. Maleki, G. Pacchioni, Steric and Orbital Effects Induced by Isovalent Dopants on the Surface Chemistry of ZrO₂, *ACS Catal.* 11 (2021) 554–567, https://doi.org/10.1021/ACSCATAL.0C04553/SUPPL_FILE/CS0C04553_SI.001.PDF.
- [61] S. Kouva, J. Andersin, K. Honkala, J. Lehtonen, L. Lefferts, J. Kanervo, Water and carbon oxides on monoclinic zirconia: experimental and computational insights, *Phys. Chem. Chem. Phys.* 16 (2014) 20650–20664, <https://doi.org/10.1039/C4CP02742F>.
- [62] S. Li, Y. Wang, B. Yang, L. Guo, A highly active and selective mesostructured Cu/AlCeO catalyst for CO₂ hydrogenation to methanol, *Appl. Catal. A Gen.* 571 (2019) 51–60, <https://doi.org/10.1016/J.APCATA.2018.12.008>.